AFRL-AFOSR-UK-TR-2023-0040

Mach number independent hot-wire anemometry

Pierre Dupont
UNIVERSITE D'AIX MARSEILLE
58 BOULEVARD CHARLES LIVON
MARSEILLE, , 13007
FRA

02/23/2023
Final Technical Report

Air Force Research Laboratory
Air Force Office of Scientific Research
European Office of Aerospace Research and Development
Unit 4515 Box 14, APO AE 09421

REPORT DOCUMENTATION PAGE

PLEASE DO NOT RETURN YOUR FORM TO THE ABOVE ORGANIZATION.

1. REPORT DATE	2. REPORT TYPE	3. DATES COVERED	
20230223	Final	START DATE 20200930	END DATE 20221031

4. TITLE AND SUBTITLE
Mach number independent hot-wire anemometry

5a. CONTRACT NUMBER	5b. GRANT NUMBER	5c. PROGRAM ELEMENT NUMBER
	FA8655-20-1-7040	
5d. PROJECT NUMBER	**5e. TASK NUMBER**	**5f. WORK UNIT NUMBER**

6. AUTHOR(S)
Pierre Dupont

7. PERFORMING ORGANIZATION NAME(S) AND ADDRESS(ES)
UNIVERSITE D'AIX MARSEILLE
58 BOULEVARD CHARLES LIVON
MARSEILLE 13007
FRA

8. PERFORMING ORGANIZATION REPORT NUMBER

9. SPONSORING/MONITORING AGENCY NAME(S) AND ADDRESS(ES)	10. SPONSOR/MONITOR'S ACRONYM(S)	11. SPONSOR/MONITOR'S REPORT NUMBER(S)
EOARD UNIT 4515 APO AE 09421-4515	AFRL/AFOSR IOE	AFRL-AFOSR-UK-TR-2023-0040

12. DISTRIBUTION/AVAILABILITY STATEMENT
A Distribution Unlimited: PB Public Release

13. SUPPLEMENTARY NOTES

14. ABSTRACT
A comprehensive characterization of the thermal response of nanoscale hot-wire probes is performed in both subsonic and supersonic flows. A constant current anemometer was designed for the measurement of the intrinsic thermal inertia of hot-wire probes. In particular, the nanoscale probe is considered with the effect of gold-plating on supporting structure of the targeted sensing element. Gold-plated nanoscale probes present a response time one order of magnitude smaller than conventional cylindrical hot-wire probes. Heat transfer simulations show that the temperature profile is considerably modified by the addition of a conductive metal layer, hence increasing the sensor's frequency response in both subsonic and supersonic flows. The increase of frequency response is finally exemplified by the numerical computation of the power spectral density of a turbulent flow signal without any electric compensation of the hot-wire signal.

15. SUBJECT TERMS

16. SECURITY CLASSIFICATION OF:			17. LIMITATION OF ABSTRACT	18. NUMBER OF PAGES
a. REPORT U	b. ABSTRACT U	c. THIS PAGE U	SAR	17

19a. NAME OF RESPONSIBLE PERSON	19b. PHONE NUMBER *(Include area code)*
DOUGLAS SMITH	314 235 6013

Standard Form 298 (Rev.5/2020)
Prescribed by ANSI Std. Z39.18

FINAL REPORT

AFOSR grant number FA8655-20-1-7040
Mach-number independent hot-wire anemometry

February 8, 2023

F. Brunier-Coulin, D.C. Barros, M. Hultmark and P. Dupont

Contents

1 PREFACE

This manuscript is the final report of the grant number FA8655-20-1-7040 monitored by Dr. Douglas Smith. The investigation results from a collaboration between Aix-Marseille Université and Princeton University. Florian Brunier-Coulin is the Postdoctoral Research Associate conducting the research experiments. He is supervised by Diogo C. Barros (Assistant Professor, Aix Marseille Université, CNRS, IUSTI Laboratory), Marcus Hultmark (Associate Professor, Princeton University) and Pierre Dupont (Aix Marseille Université, CNRS, IUSTI Laboratory).

A systematic characterization of the response time of nanoscale anemometry probes is considered in both subsonic and supersonic flows. The main result at the current stage of the project is the addition of gold layers over the supporting structure of the nanoscale sensing element, which leads to a significant decrease of the response time of the probe, reaching a cut-off frequency thirty times larger than classical cylindrical wires. The response is modeled by a first-order system, which allows numerical compensation of nanoscale probe signals acquired without any electronic compensation with a constant current anemometer system. The compensated power spectral density of a high-speed turbulent signal was resolved until 100kHz, demonstrating a huge potential for next generation hot-wire anemometry in a variety of flow conditions.

2 INTRODUCTION

Hot-wire anemometry has been widely employed for unsteady flow characterization since the pioneering investigation of King [1914]. The small dimension of micron-sized wires makes them ideal for pointwise measurements in turbulent flows, both in subsonic and supersonic flow applications [Kovasznay, 1950, Comte-Bellot, 1976].

The governing principle of hot-wire anemometry relies on the thermal equilibrium between the heat generated from Joule effect and the power loss from the mean convective heat transfer to the flow:

$$R_w I^2 = hA\left(T_w - T_r\right). \tag{1}$$

In this relation, R_w and I stand for the electrical wire resistance and traversing current, respectively; h is the convective heat transfer coefficient and A the wire surface exposed to the flow. T_w and T_r are defined as the mean wire and recovery temperatures, respectively. While equation (1) allows one to compute the heat loss and to scale it with the mean flow velocity, it remains crucial to determine the transient thermal response of the wire to evaluate any spectral or statistical properties of both velocity and temperature fluctuations.

The current work provides a systematic characterization of the frequency response of nanoscale hot-wire probes by the use of an in-house constant current anemometry system. A step change of electric current traversing the hot-wire is considered, and the corresponding thermal response associated with a change of the wire's voltage was quantified in both subsonic and supersonic flow conditions for multiple wire temperatures.

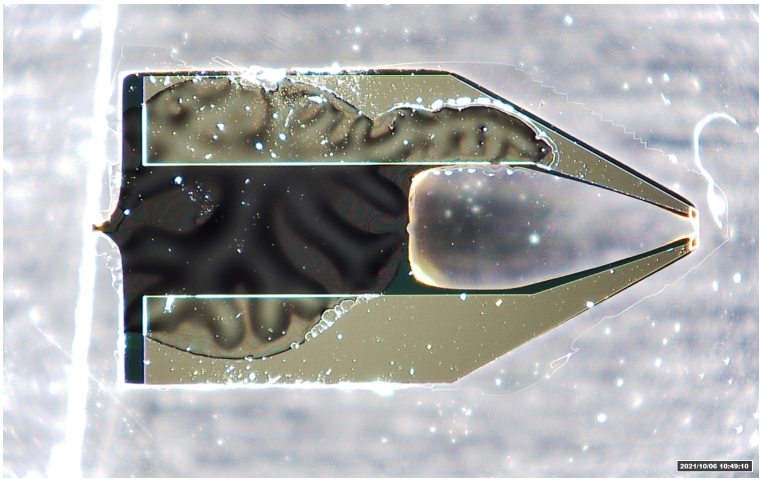

Figure 1: NSATP probe after fabrication in the Princeton Nano-Fabrication laboratory.

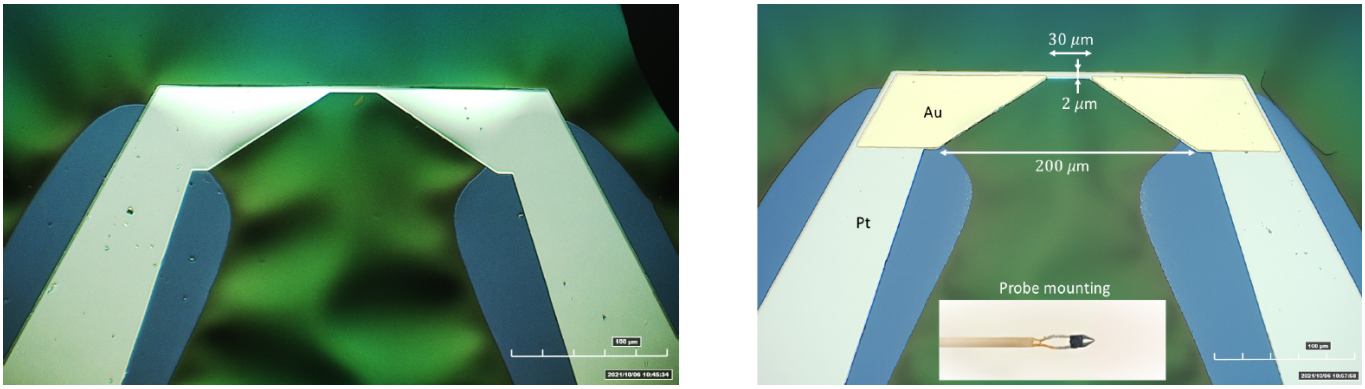

Figure 2: Left: platinum sensor; right: gold-plated platinum probe with gold thickness of 360 nm .

3 NANOSCALE ANEMOMETRY PROBES

The novel fabrication methods in microelectromechanical systems (MEMS) paved the way for the design of hot-wire probes targeting highly resolved measurements in a variety of flow conditions [Vallikivi and Smits, 2014, Kokmanian et al., 2019, Le-The et al., 2021]. In particular, nanoscale thermal anemometry probes (NSTAP) consisting of ribbons with thickness of 100-300 nm one order of magnitude smaller than classical hot-wire cylindrical probes show a huge potential for time-resolved measurements even in high-speed flows [Kokmanian et al., 2021]. Figure 1 illustrates a platinum nanoscale probe after production.

In figure 2(left), we depict the details of the geometry around the nanoscale sensing element. Their platinum structure is composed of main large supports converging to the 30 μm-long sensing ribbon element with thickness of 300 nm and width 2 microns. The triangular supports adjacent to the sensing element are supposed to impact significantly the thermal response of the entire sensor. In order to modify the thermal response of these supports, layers of gold were added specifically to the wire supports as depicted in figure 2(right). The goal of adding the gold layer is twofold: to increase the electrical conductivity and the support cross section consequently reducing the Joule effect, and to increase heat conductivity to reduce the temperature gradient across the supporting structure. This effect would reduce

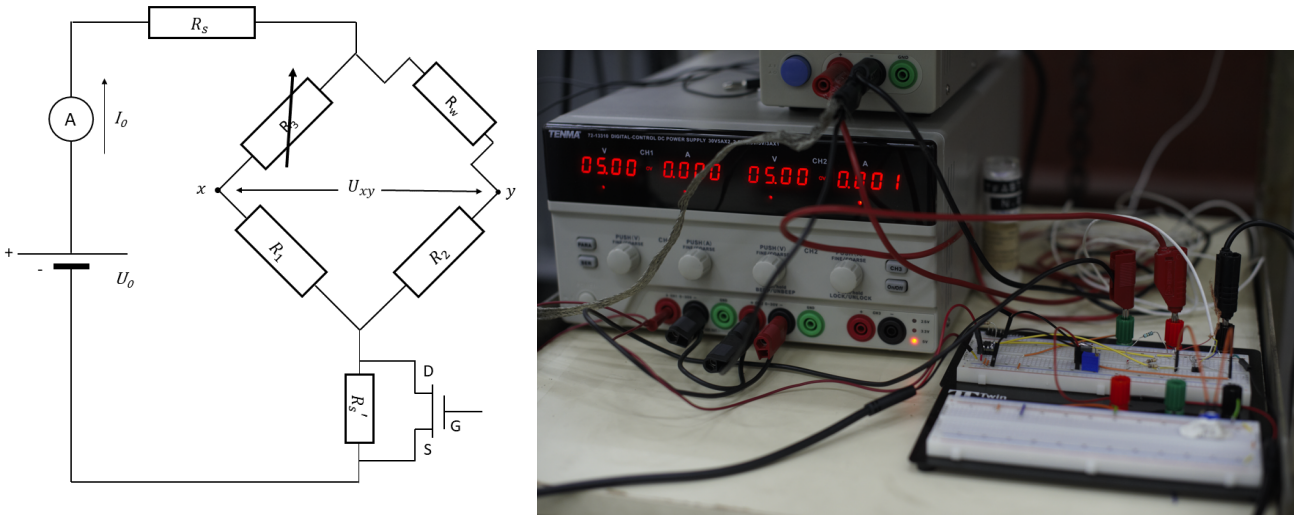

Figure 3: Electronic device sketched on the left and captured during the Square Wave Test measurement on the right.

the thermal response time of the entire sensor. In the following, two gold-plated configurations with thickness 200 nm and 360 nm will be considered. All the fabrication steps of the sensors are described in Kokmanian et al. [2019].

4 RESPONSE TIME MEASUREMENTS

The time constant τ of the sensors can be experimentally measured by the implementation of a square wave test. The method consists in simulating a step change of the flow velocity by a step variation of the electric current traversing the wire [Bruun, 1995]. The wire's voltage follows a first order linear system response:

$$E = C\left(1 - e^{-\frac{t}{\tau}}\right), \tag{2}$$

where E is the instantaneous bridge voltage. During the square wave test, the probe is placed in stabilized flow conditions, and the wire is one of the electric resistances of a balanced Wheatstone bridge fed by a constant current. A sketch of the circuit is presented in figure 3.

We simulate a periodic, step response of the flow velocity by a square wave signal generated by a Mosfet transistor component which periodically short-circuits the small resistance ($R_s{}'$ (bottom of figure 3). The variable resistance R_3 in parallel to the sensor's resistance (R_w) allows one to set the overheat ratio $a_w = (R_w - R_e)/R_e$ of the wire, where R_e is the equilibrium resistance of the wire in the current flow conditions without heating. The quasi-periodic wire voltage response was measured using a 8-bit scope and phase-averaged to obtain the response time τ.

The experiments were conducted in multiple flow conditions, spanning from the subsonic to supersonic flow regimes. For the low-speed configuration, a circular jet issuing from a nozzle with diameter 3 cm was employed to characterize the frequency response in the subsonic regime. The jet exit velocity

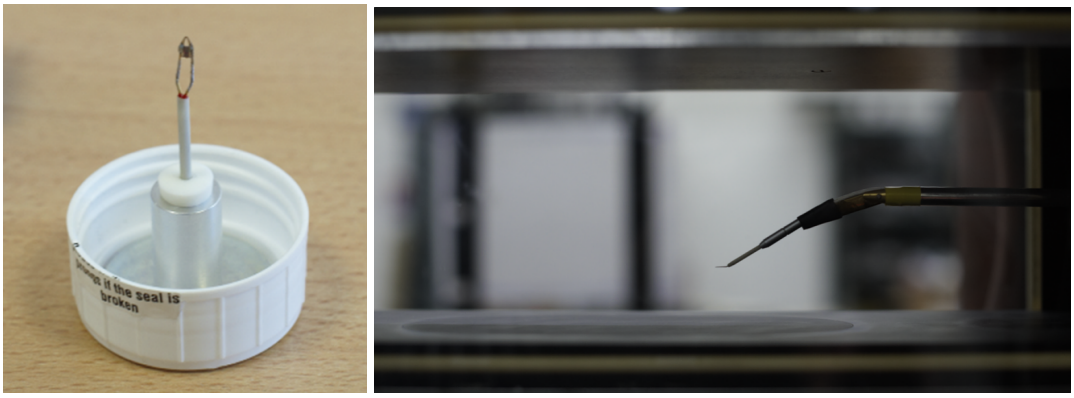

Figure 4: Probe mounted in the potential core of the flow in the supersonic wind tunnel.

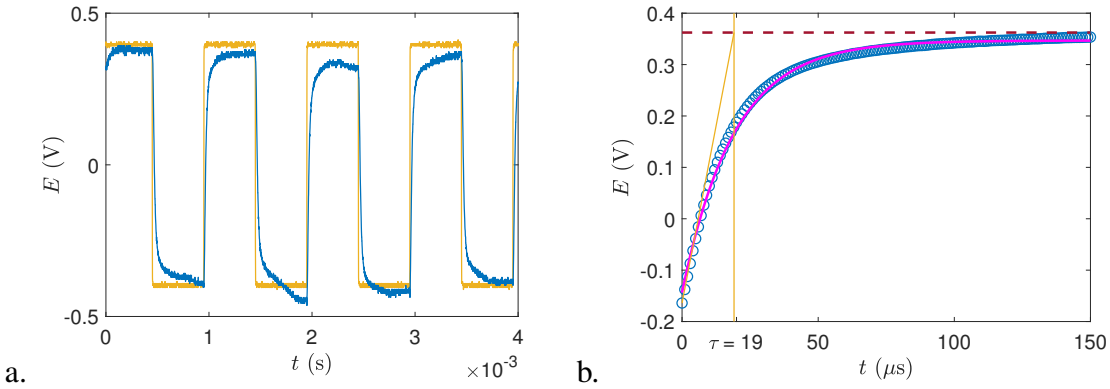

Figure 5: a) Response of the NSTAP sensor (blue) to the square wave test (yellow) applying step changes of the electric current. b) Phase-averaged wire voltage response and exponential fit to compute the time constant τ using equation 2. In the current example, the time constant was found to be $\tau = 19\,\mu$s.

was $7\,$m$/$s, and the probe was placed at the potential core of the jet. To measure the response time in high-speed conditions, the probe was placed in the free-stream flow issuing from a Mach 2 rectangular nozzle in a continuous supersonic wind-tunnel with very low turbulence level. Figure 4 shows the nanoscale probe installed with the prongs in the wind-tunnel test section. All the experiments were conducted at the Institut Universitaire des Systèmes Thermiques et Industriels (IUSTI, Marseille).

Figure 5(left) presents an example of the wire voltage response to a square wave step current corresponding to $\Delta I = 0.04 \times I$. In figure 5(right), we depict the phase-averaged response fitted with the exponential growth from equation 2. The time constant τ corresponds to the intersection between the first slope and the asymptotic value.

In figure 6, we compare the response time of multiple sensors for various overheat resistance coefficients a_w, including a classical 5 μm-cylindrical hot-wire, the platinum-based and the gold-plated nanoscale sensors with different layer thicknesses in both subsonic and supersonic flow conditions. Noticeably, the response time of the nanoscale sensors is at least five times lower than the classical $5\,\mu$m-tungsten wire for both subsonic and supersonic configurations. Interestingly, the addition of gold layers monotonically decreases the response time up to $\tau \sim 20\,\mu$s. The trends are the same whether the probe is placed in low or high-speed flows. The response time of nanoscale sensors is almost constant for variable

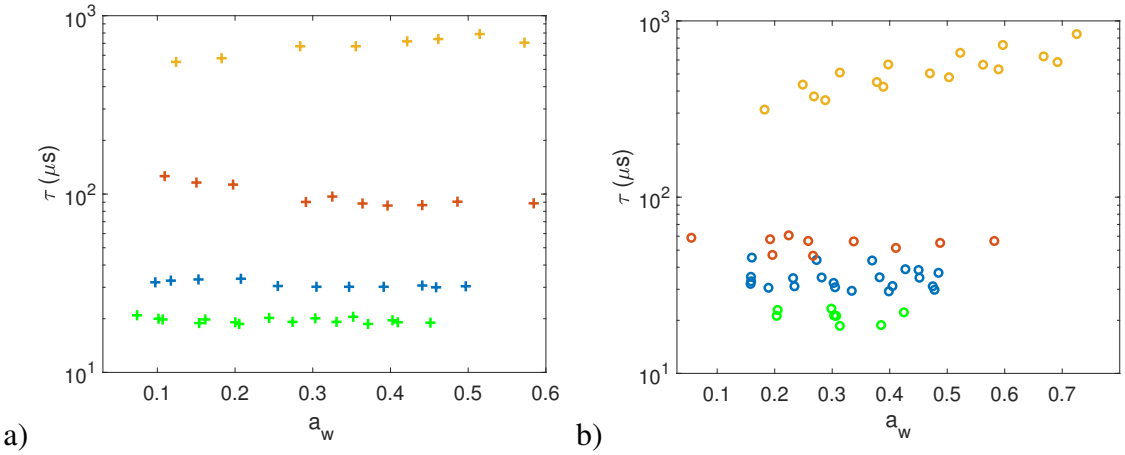

Figure 6: Time constant measured in subsonic (a) and supersonic (b) flows for a classical 5 μm Dantec cylindrical wire (yellow), the NSTAP without gold (red), NSTAP with 200 nm gold layer (blue) and NSTAP with 360 nm gold layer (green). Vertical error bars can be considered smaller than 10% in subsonic and smaller than 5% in supersonic configurations.

Table 1: Averaged τ (μs) over a_w in subsonic and supersonic flows.

Sensor	Subsonic	Supersonic
5 μm cylindrical wire	678.7	526.3
NSTAP platinum	98.3	54.6
NSTAP platinum + 200 nm of gold	35.9	34.2
NSTAP platinum + 360 nm of gold	19.6	19.5

overheat coefficients a_w. The lowest response time $\tau = 20\,\mu$s was obtained for a gold-plated nanoscale probe with gold layer of 360 nm, corresponding to a reduction by a factor of 30 of the response time when compared to a classical 5 μm-tungsten wire.

In table 1, we summarize the values of τ averaged over a_w according to both the sensor and the flow configurations. We note that τ generally reduces for higher flow speeds, a fact that can be predicted from the unsteady heat equation over the probe [Bruun, 1995]. This reduction, however, is negligible for the gold-plated NSTAP sensors. A detailed knowledge of the sensing element's resistance would be crucial to understand why the response time remains unchanged for subsonic and supersonic flow conditions when the gold layers are added.

Another point of interest is the effect of the flow condition associated with the overheat ratio on the response time. Although limited measurements were performed for supersonic flow conditions, figure 7 depicts the response time for both the conventional cylindrical and a gold-plated NSTAP for varying flow speed (i.e. total pressure P_0) and overheat ratio a_w. The 5 μm-probe presents a linear growth with a_w for both flow speeds. It is interesting to note that for increasing a_w, there is a decrease of the response time when the flow speed rises. Both the linear growth of τ with a_w and the nonlinear decrease of τ with flow speed can be predicted using a simple heat transfer model of a cylindrical hot-wire probe [Bruun, 1995]. On the other hand, the gold-plated NSTAP probe presents no a_w dependence within the

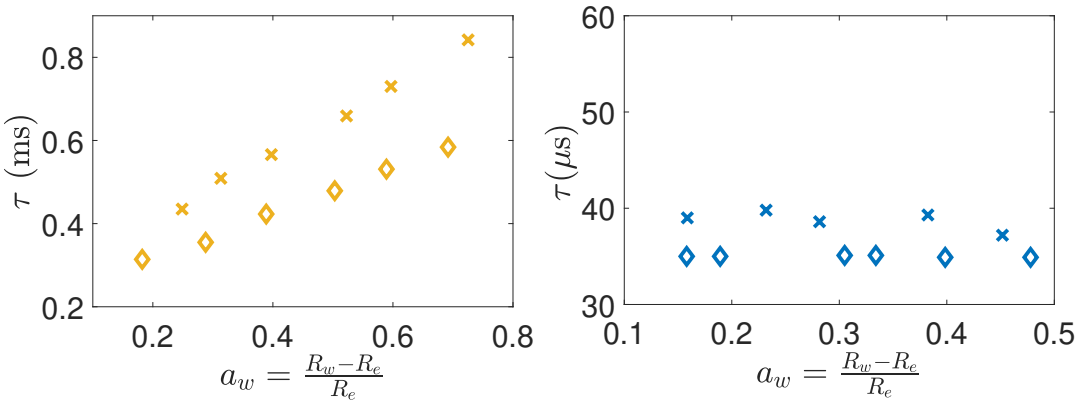

Figure 7: Time constant evolution in supersonic flow as a function of the overheat ratio a_w for the classical 5 μm probe (left) and for the gold-plated NSTAP with a 200 nm gold layer (right) at different total pressure levels: open diamonds stand for $P_0 = 0.8$ bar and crosses stand for $P_0 = 0.4$ bar.

measurement uncertainties, but a decrease of τ with flow speed. While this behavior would be beneficial for experimental purposes and robustness to a_w variations, the physical reasons behind the difference between the cylindrical and the NSTAP probes remains to be elucidated.

5 HEAT TRANSFER ANALYSIS

5.1 Theoretical model

In CCA operation without electronic compensation, the time constant is governed only by the thermal inertia of the sensor. The effect of the gold plating on the probe temperature profile is explored here using a heat transfer model and corresponding numerical simulations. In particular, we attempt to characterize how the temperature gradient changes in the vicinity of the sensing element.
To understand the heat transfer mechanisms leading to a reduction of the response time by the addition of gold, we conduct a thermal analysis considering the heat fluxes at play in the problem.

The heat transfer balance for the hot-wire sensor can be written as :

$$d\dot{Q}_p = d\dot{Q}_h + d\dot{Q}_k + d\dot{Q}_s, \tag{3}$$

where $\dot{Q}_p$ is the generated heat by Joule effect and $\dot{Q}_s$ is the power absorbed by the wire element. $\dot{Q}_h$ and $\dot{Q}_k$ stand for the heat exchange by convection and conduction, respectively.

Let A be the wire cross-section and k_w its thermal conductivity, C_p its heat capacity, ρ the wire density and χ_0 the resistivity at the temperature T_0, equation 3 writes:

$$\frac{\chi_0 I^2}{A} = \left(\pi k_a Nu - \frac{\chi_0 I^2}{A}\alpha_0\right)\theta - k_w A\frac{\partial^2\theta}{\partial x^2} + \rho C_p A\frac{\partial\theta}{\partial t}. \tag{4}$$

Here, θ is the temperature variation $T(x) - T_0$, k_a is the air thermal conductivity and Nu the Nusselt number. The Nusselt number is usually a function of the Reynolds and Mach numbers. In subsonic conditions, it is known as the King's law $Nu = A\sqrt{Re} + B$.

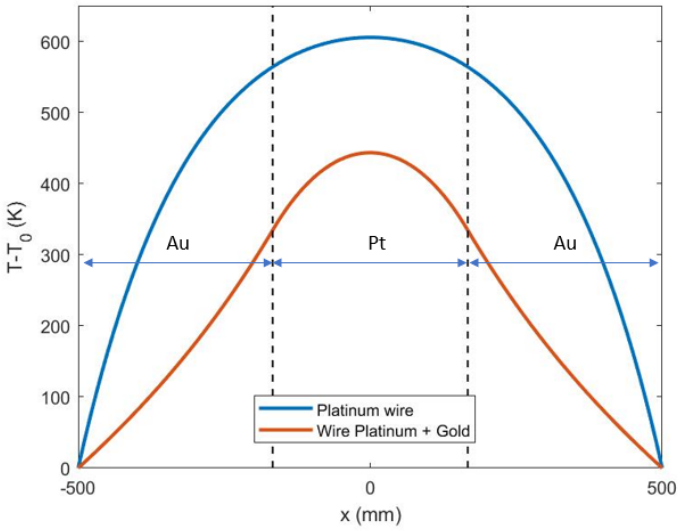

Figure 8: Analytic profile of temperature along a platinum wire of 5 μm diameter (blue curve) and same wire dimension with gold instead of platinum on 350 μm long on both ends (orange curve)

The model can be solved analytically considering the equilibrium steady state ($\frac{\partial \theta}{\partial t} = 0$):

$$\theta(x) = C_1 \exp(\lambda x) + C_2 \exp(-\lambda x) + F \tag{5}$$

with

$$\lambda = \frac{\sqrt{A k_a \pi N u - I^2 \chi_0 \alpha_0}}{A\sqrt{k_w}}$$

$$F = \frac{I^2 \chi_0}{A k_a \pi N u - I^2 \chi_0 \alpha_0}$$

C_1 and C_2 are constants obtained from the boundary conditions.
Let us consider a 5 μm-diameter cylindrical platinum wire with length 1 mm. The temperature distribution along the wire can be calculated using equation (5) with appropriate flow conditions. This profile is presented in figure 8. We also plot the effect of the replacement of platinum by gold at the two extremities of the sensor. It is noticeable using this simple model how the temperature decreases by the addition of a material with larger thermal conductivity and lower resistivity.

The geometry of the nanoscale sensors investigated in the current work is, of course, far from being a simple cylindrical wire. To shed further light on the temperature profile along the nanoscale sensor, we employed an infra-red thermal camera FLIR fitted with a microscope lens giving a resolution of 10 μm/pixel. This resolution is not sufficient for a reliable quantitative analysis of the temperature profile along the sensing element. However, the contour plot of temperature shown in figure 9(left) clearly indicate an increase of the temperature along the triangular structure supporting the sensing element.

The analysis has been extended to the actual geometry of the NSTAP's probes (see)Brunier-Coulin et al. [2022]).

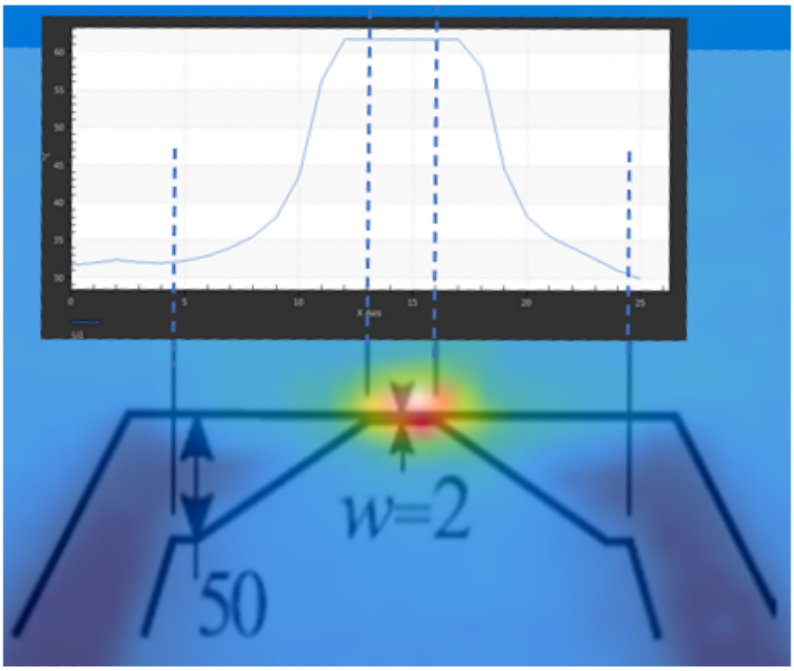

Figure 9: Qualitative temperature profile along te NSTAP platinum sensor using an infra-red thermal camera.

We consider a one-dimensional model along the sensor's length axis x following Bruun [1995]. The equilibrium between the electrical heat generated by the Joule effect $\dot{Q}_e$ and the heat exchange by conduction $\dot{Q}_c$ and convection $\dot{Q}_h$ will be expressed for an incremental sensor element.
The generated heat by the traversing electric current I is given by:

$$d\dot{Q}_e = dR_w I^2 = \frac{\chi_w(x,T(x))I^2}{A(x)}dx. \tag{6}$$

Here, $\chi_w(x,T)$ and $A(x)$ are the local electrical resistivity and cross section of the sensor, respectively, while $T(x)$ is the local wire temperature. The local resistivity χ_w is modelled by introducing the thermal coefficient of resistance α_0 and the resistivity χ_0 at $T_O = T_{293K}$:

$$\chi_w(x) = \chi_0\{1+\alpha_0[T(x)-T_0]\}. \tag{7}$$

The heat convection from the wire to the flow is governed by the heat transfer coefficient, h, acting on the external surface S_w:

$$d\dot{Q}_h = h(x)S_w[T(x)-T_e]\,dx. \tag{8}$$

We consider $S_w = 2[w(x)+t]$ which takes into account both the upper and lower surfaces of the rectangular structure of the sensor.

Thermal conduction along the sensor is considered in the axial direction:

$$d\dot{Q}_c = -k_w A(x)\frac{\partial^2 T(x)}{\partial x^2}dx \tag{9}$$

and the heat storage is written as

$$d\dot{Q}_s = \rho_w C_p A(x) \frac{\partial T(x)}{\partial t} dx. \tag{10}$$

In the equations above, the density and heat capacity of the sensor's material are respectively ρ_w and C_p; the thermal conductivity is k_w. The equilibrium temperature of the unheated wire is T_e. Finally, the local width, the local cross-section and the sensor's thickness are $w(x)$, $A(x)$ and t, respectively.

5.2 Numerical simulation

The stationary solution of equations 10 provides the temperature profile across the sensing element and its vicinity. The problem consists in solving the heat transfer equations accounting for the geometry and materials of both a conventional cylindrical wire and the NSTAP sensors, which are sketched in figure 10. A Neumann condition is applied at the center of the wire, and the equilibrium temperature T_e is imposed at both extremities of the sensor. The equations were solved using the Finite Element Method (FEM), where the probe geometry was discretized in 1300 nodes. The sensor is surrounded by a low-speed air flow with free-stream velocity $u = 5$ m/s.

The convective heat transfer coefficient is modeled using a local Nusselt number:

$$h(x) = Nu \frac{k_f}{\ell(x)}, \tag{11}$$

where k_f is the fluid thermal conductivity and $\ell(x)$ the characteristic length scale in the flow direction. For a cylindrical wire, we set $\ell(x) = d$. For the ribbon shape of the NSTAP, we follow Kokmanian et al. [2021] who considered both the width $w(x)$ and the thickness t. As the width w can be much larger than t and parallel to the fluid flow, we expect the most appropriate length scale $\ell(x) = w(x)$, which varies from 2 μm at the tip until approximately 50 μm at the vicinity of the sensing element (see figure 3 for the sensor's geometry). The Nusselt number employed here follows the King's law $Nu = A\sqrt{Re} + B$, with coefficients $A = 0.43$ and $B = 0.32$ empirically obtained for cylindrical hot-wires [McAdams, 1954]. Here, the Reynolds number $Re = ul(x)/\nu$ is computed with the length scale $\ell(x)$ and the mean flow speed u of air with kinematic viscosity ν.

The numerical model was first validated with the cylindrical 5 μm-tungsten wire. The temperature distribution along the wire axis $T(x)$ is shown in figure 5.2 for an arbitrary overheat ratio and electric power. The temperature profile agrees well with previous theoretical predictions examined in Bruun [1995]. The mean temperature of the wire obtained numerically was $\langle T_w \rangle_{num} = 516K$. while the estimated temperature from the experiments was $\langle T_w \rangle_{exp} = 478K$. This difference might come from the experimental estimation that uses the measured wire resistance to compute the wire temperature:

$$\langle T_w \rangle_{exp} = \frac{R_w - R_e}{R_0 \alpha_0} + T_e \tag{12}$$

The model uses the resistivity of the wire to calculate the wire temperature that is integrated over the sensor's length.

To understand the effect of gold-plating on the heat transfer across the wire, simulations were performed for the NSTAP sensors matching the experimental conditions $I = 10$ mA for the platinum probe and $I = 12$ mA for the 360 nm gold plated sensor. These values correspond to the experiments conducted

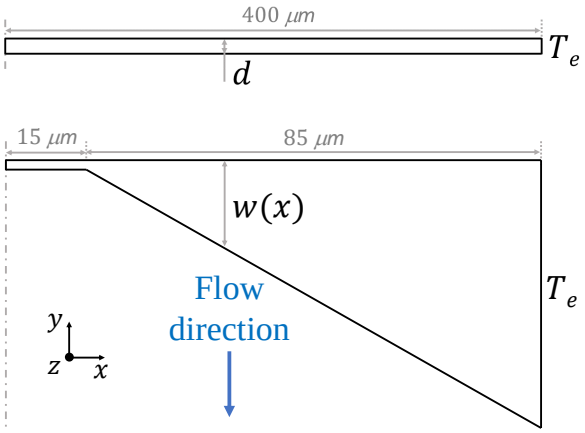

Figure 10: Geometry of the cylindrical tungsten wire (d =5 μm, top) and the nanoscale probe (bottom) considered in the numerical simulations.

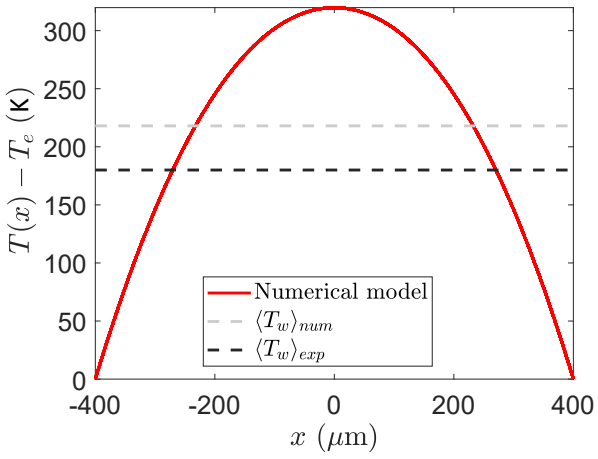

Table 2: Thermal and physical properties of materials at 293 K.

Mat.	C_p $[J.kg^{-1}.K^{-1}]$	ρ_w $[kg.m^{-3}]$	k_w $[W.m^{-1}.K^{-1}]$
Pt	130	21450	71.6
Au	128	19300	320
W	203	15630	174

Table 3: Electric properties of the sensor's materials at 293 K.

Mat.	χ_0 $10^{-6}[\Omega.m]$	α_0 $10^{-3}[K^{-1}]$
Pt	0.1111	3.92
Au	0.0222	3.71
W	0.1124	3.68

in the potential core of a jet with maximum flow speed $u = 5$ m.s^{-1}, coresponding to $R_w I^2 \simeq 3.8$ mW and $a_w \simeq 0.2$. For simplicity, only one half of the sensing element is solved as sketched in figure 10.

Figure 11 depicts the temperature profile $T(x)$ along the center-axis of the NSTAP probes. To better contrast the effects of gold on the temperature profile, we normalize $T(x) - T_e$ by the average temperature of the sensing element (*i.e.* for $0 \leq x \leq 15$ μm for the half-sensor) subtracted by T_e. Without the presence of the gold layer, the curve presents a substantial sensor heating along the triangular structure ($15 \leq x \leq 100$ μm), which is highly attenuated by the presence of the 360 nm-metal layer. Hence, gold-plating mostly focuses the temperature gradient along the sensing element which directly reduces the response time of the sensor.

It is interesting to inquire to what extent this temperature profile is associated with end-conduction effects of the probe. For a cylindrical hot-wire, these effects can be quantified using the Γ parameter proposed by Hultmark et al. [2011], which is defined based on the length-to-diameter ratio, the resistance ratio $a = R_w/R_e$, the Nusselt number Nu, the wire and the fluid thermal conductivity k_w and k_f, respectively. For the nanoscale ribbon geometry investigated here, the parameter assumes the following form [Byers, 2018]:

$$\Gamma = \frac{l}{w}\sqrt{2a\left(\frac{k_f}{k_w}\right)\left(\frac{w+t}{t}\right)Nu} \tag{13}$$

where l, w and t stand for the length, the width and the thickness of the ribbon sensing element. Preliminary estimations of the Nusselt number reported by Kokmanian et al. [2021] indicate $Nu \sim \mathcal{O}(50)$, which would lead to a Γ parameter insufficiently small to avoid end-conduction effects. An extensive characterization of the end-conduction effects for the present nanoscale geometry is hence necessary in future work, taking into consideration the exact values of the sensing element resistance, in spite of the entire probe impedance.

To localize the heat transfer on the sensing element, it is necessary to reduce the electrical heat production of the ribbon structure. As the heat production is proportional to $R_w I^2$, one would consider to reduce the local resistivity χ by adding a parallel conductor, here the gold-layer with thickness similar to the platinum structure. The gold-layer reduces the global resistivity by a factor $2\chi_{Au}/(\chi_{Pt} + \chi_{Au}) \simeq 0.33$. In addition, the thermal conductivity of the sensor is increased by a factor of almost 3 reducing the

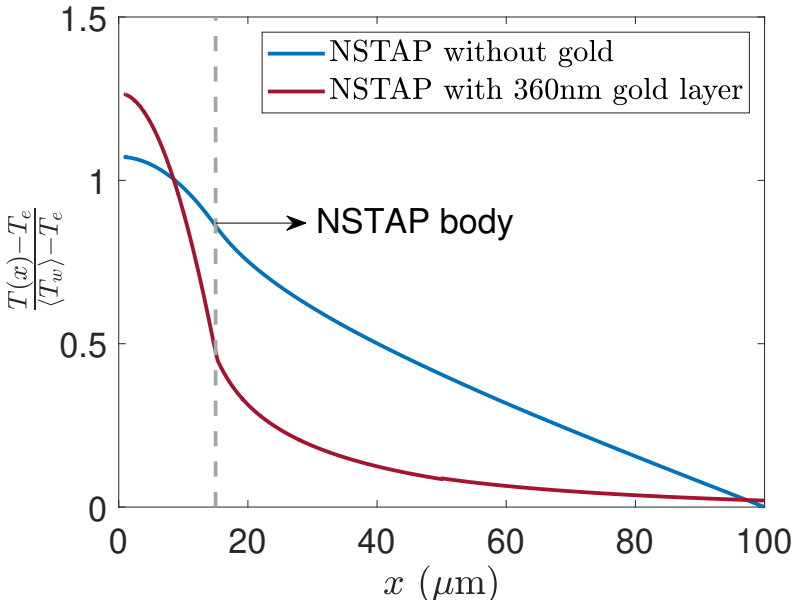

Figure 11: Comparison of the numerical profile $T(x) - T_e$ normalized by the mean temperature of the sensing element $\langle T_w \rangle - T_e$ along the half length of the sensor with and without gold plating. The dashed line represent the limit between the ribbon-shaped sensing element and the supporting triangular structure.

temperature variation between both extremities of the triangular supports at a constant heat production. The properties of all materials are presented in tables 2 and 3.

6 NUMERICAL COMPENSATION OF A TURBULENT FLOW SIGNAL

The addition of gold to the supporting structure focuses the temperature gradient into the sensing element, lowers the temperature of the stubs, hence reducing the response time of the probe. The decrease of the response time by an order of magnitude is associated with an equivalent increase of the sensor's frequency response. While in conventional operation of hot-wire probes in both CTA and CCA systems the signals are compensated with a parallel electronic circuit, one could inquire to what extent numerical compensation using the analytical first-order transfer function would provide reliable power spectral density results for the use of nanoscale probes in turbulent flows.

Given that the phase-averaged response signals show unambiguously the first-order nature of the sensor's response, the probe transfer function can be modeled as a low-pass filter. This is governed by the well-known transfer function:

$$H(j\omega) = \frac{1}{1 + j\frac{\omega}{\omega_o}}. \tag{14}$$

ω is the angular frequency and ω_0 is the cut-off angular frequency defined as $\omega_0 = 1/\tau$. The resulting cut-off frequency is given by $f_0 = \omega_0/2\pi$. The transfer function gain G is the magnitude $\|H(j\omega)\|$. Using

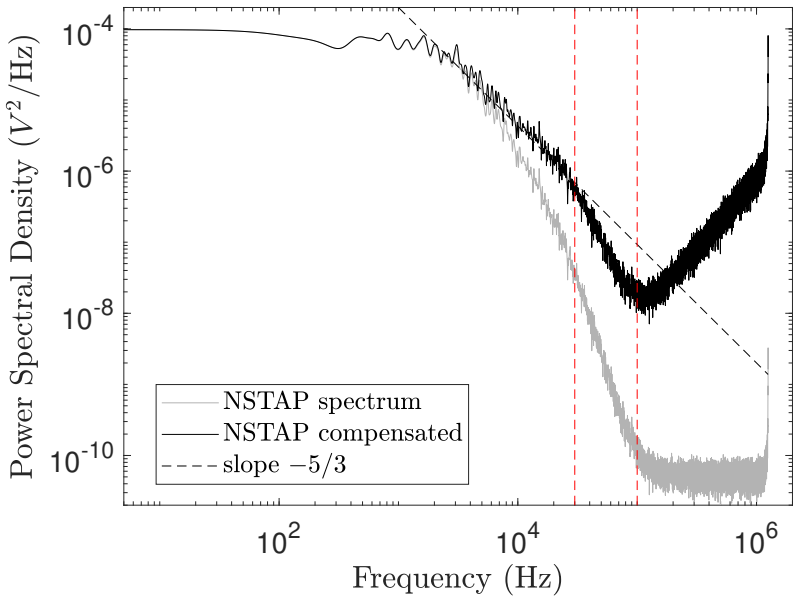

Figure 12: Spectrum of the NSTAP with a gold layer of 200 nm. Red dashed lines represent the dissipation range and the cut-off frequency after compensation.

the conventional frequency variable $f = \omega/2\pi$, the frequency-dependent gain is computed as:

$$G(f) = \frac{1}{\sqrt{1+(f/f_0)^2}} \tag{15}$$

For a given power spectral density of a turbulent flow signal acquired without compensation, the compensated power spectral density S_i is computed by the ratio between the measured power spectral density S_o and the squared gain $G(f)^2$.

To experimentally test the numerical compensation of a turbulent flow signal, the gold-plated nanoscale probe was placed in a high-subsonic jet issuing from a nozzle with an exit internal diameter $D_i = 4$ mm. The estimated jet flow speed based on static and stagnation pressure is $v = 105$ m/s. During the measurements, the probe was placed within the jet shear layer approximately four diameters downstream of the nozzle's outlet.

The power spectral density of hot-wire signals in this location should exhibit the universal $k^{-5/3}$ decay for more than one decade [Proença et al., 2019]. Figure 12 presents the power spectral density (PSD) of both the original and the numerically compensated signals. It is important to note that the original signal was acquired using the CCA anemometer system described in section **??** without any compensation. Hence, in the PSD of the original signal, the rapid decay starting at approximately 4 kHz is due to the intrinsic thermal response of the nanoscale probe. This cut-off frequency agrees well with the response time $\tau = 30 - 40\,\mu$s presented in figure 5 for the 200 nm gold-plated probe. The compensated PSD shows a compelling $k^{-5/3}$ decay until 30 kHz where turbulent flow dissipation increases the decay rate until 100 kHz, which is the cut-off frequency of the compensated signal limited by the signal's noise originated from a digital converter of $N = 16$ bits.

7 CONCLUSIONS AND OUTLOOK

A constant current anemometer was built to characterize systematically the response time of nanoscale probes under multiple aerodynamic and overheat configurations. The experimental results show that the NSTAP probes present a response time at least one order of magnitude smaller than conventional cylindrical hot-wire probes. The associated frequency response shows similar features whether the probe is placed in subsonic or supersonic flow conditions, thus confirming the possibility of using the nanoscale probes in a variety of Mach number flows. It was shown that the time constant of the NSTAP sensors is insensitive to the overheat ratio, which is in contrast to the behavior of conventional hot-wire probes.

To explore the effects of the supporting structure on the sensor's frequency response, a gold layer was added at the vicinity of the sensing element over the original platinum structure. t demonstrates the possibility to control the response time by gold-plating, which focuses heat transfer along the nanoscale sensing element. The addition of gold-plating at the vicinity of the sensing element deserves further detailed investigations to find an optimal configuration considering both the response time and the end-conduction effects.

Finally, numerical compensation of acquired CCA signals without any electric compensation was successfully implemented in a high-speed turbulent flow. Due to the higher frequency response of the probe when compared to conventional hot-wires, the power spectral density of a turbulent flow signal can be computed over a large range of frequencies, which are limited only by the intrinsic noise of the acquisition system. In the tested experiments, a gold-plated nanoscale probe covers a spectral range until 100 kHz, paving the way for its application in a variety of flow conditions without the need of any sophisticated anemometer system with electric compensation.

The results obtained in the present project show that the NSTAP technology is now mature to be used in a large variety of flows: from subsonic to high-speed flows. Their exceptional low time constant suggests that the design of a low-noise constant current anemometer for the operation of NSTAP probes should be quite easy to achieve. Some points have to be further investigated. First of all, the precise evaluation of the resistance of the active element, which defines the exact overheat ratio used, has to be improved. The second point is to used th results obtained during this project to design specific probes for high speed flows, limiting the rarefied gaz effects around the probe but maintaining a low time constant. This could be obtained using the large possibilities offer by the NSTAP manufacturing technology which allow to separate the thickness of the sensitive element from its longitudinal extent. This will require new sensor design and toi evaluate the associated new time constants and aerodynamic sensitivities. If both parameters (reduced timle constant and no-rarefied gaz effcets) could be achieved, this would lead to a new anemometer generation with never obtained bandwidth together an easy calibration procedure and high signal to noise ratio. This would open new experimental possibilities for basic and applied studies in laminar to turbulent high speed flows.

References

L.V. King. On the convection of heat from small cylinders in a stream of fluid: Determination of the convection constants of small platinum wires with applications to hot-wire anemometry. *Philosophical transactions of the royal society of London. series A, containing papers of a mathematical or physical character*, 214(509-522):373–432, 1914.

L.S.G. Kovasznay. The hot-wire anemometer in supersonic flow. *Journal of the Aeronautical Sciences*, 17(9):565–572, 1950.

G. Comte-Bellot. Hot-wire anemometry. *Annual Review of Fluid Mechanics*, 8(1):209–231, 1976.

M. Vallikivi and A.J. Smits. Fabrication and characterization of a novel nanoscale thermal anemometry probe. *Journal of microelectromechanical systems*, 23(4):899–907, 2014.

K. Kokmanian, S. Scharnowski, M. Bross, S Duvvuri, M.K. Fu, C.J. Kähler, and M. Hultmark. Development of a nanoscale hot-wire probe for supersonic flow applications. *Experiments in Fluids*, 60(10): 1–10, 2019.

H. Le-The, C. Küchler, A. van den Berg, E. Bodenschatz, D. Lohse, and D. Krug. Fabrication of free-standing pt nanowires for use as thermal anemometry probes in turbulence measurements. *Microsystems & Nanoengineering*, 7(1):1–11, 2021.

K. Kokmanian, D.C. Barros, M. Hultmark, and P. Dupont. Heat transfer measurements of a nanoscale hot-wire in supersonic flow. *Experiments in Fluids*, 62(8):1–13, 2021.

H.H. Bruun. Hot-wire anemometry: principles and signal analysis, 1995.

Florian Brunier-Coulin, Diogo Barros, Alexander Piqué, Marcus Hultmark, and Pierre Dupont. Thermal response of a nanoscale hot-wire in subsonic and supersonic flows. *Experiments in Fluids*, 64, 12 2022. doi: 10.1007/s00348-022-03545-z.

William H. McAdams. *Heat Transmission*, volume Chap. X. McGraw-Hill Book, 1954.

Marcus Hultmark, Anand Ashok, and Alexander J Smits. A new criterion for end-conduction effects in hot-wire anemometry. *Measurement Science and Technology*, 22(5):055401, 2011.

Clayton Phillip Byers. *Theoretical and experimental investigations of similarity solutions in turbulent flows*. PhD thesis, Princeton University, 2018.

A. Proença, J. Lawrence, and R. Self. Measurements of the single-point and joint turbulence statistics of high subsonic jets using hot-wire anemometry. *Experiments in Fluids*, 60(4):1–17, 2019.